X-RAY SPECTROMETRY
X-Ray Spectrom. 2001; **30**: 37–43

A model for low-energy thick-target bremsstrahlung produced in a scanning electron microscope

Mars Semaan[1] and C. A. Quarles[2]*

[1] Lebanese American University, Byblos, Lebanon
[2] Texas Christian University, Fort Worth, Texas 76129, USA

Received 19 January 2000; Accepted 12 October 2000

Thick-target bremsstrahlung measurements were obtained for various atomic numbers and for energies between 10 and 25 keV. A Jeol JSM 6100 scanning electron microscope was used for the electron beam and a Oxford Instruments Link Si(Li) detector for the bremsstrahlung spectrum. The experimental data were compared with a model that computes the thick-target bremsstrahlung spectrum by integrating the tabulated relativistic partial-wave doubly differential cross-section for thin-target bremsstrahlung over the target taking electron energy loss into account in the continuous slowing down approximation. The model corrects for electron backscattering, x-ray attenuation in the target and the efficiency of the x-ray detector. Very good agreement was found between the model and the experimental results. Extension of the model to consider multiple scattering in the target is also discussed. Copyright © 2001 John Wiley & Sons, Ltd.

INTRODUCTION

The production of bremsstrahlung from electron bombardment of a thick target, i.e. one in which the electrons come to rest, is a complex process. The bremsstrahlung depends, of course, on the fundamental cross-section for the interaction of an electron with an atom in the target. Electrons lose energy in the target mainly by ionization. The bremsstrahlung spectrum is composed of radiation from electrons having any energy less than or equal to the incident energy. The spectrum depends on the angle of x-ray emission and so is affected by the scattering of the electrons in the target. Ionization can produce secondary electrons that can share the projectile electron's energy and also radiate in subsequent interactions in the target. Finally, the x-rays are self-attenuated in the target and the distance of travel depends on where the electron is in the target when it radiates. The bremsstrahlung can be observed in reflection mode, where the x-rays come out of the surface initially struck by the incident electron. Alternatively, if the material is thin enough, the x-rays can be observed in transmission.

There are several advantages of the model discussed here for specific applications. A model that accurately predicts the absolute value of the bremsstrahlung background from thick targets is useful in scanning electron microscopy (SEM), energy-dispersive x-ray analysis (EDX) and electron microprobe (EPMA) applications. With accurate bremsstrahlung predictions, an independent absolute normalization of the characteristic x-ray spectra is possible. Use of a model is a compromise between a purely empirical approach and a more complex Monte Carlo approach to obtaining an accurate description of the bremsstrahlung background. This model alleviates the usual concern of an empirical technique about the validity of interpolation between the empirical benchmarks. On the other hand, the model is much simpler and quicker to calculate than the Monte Carlo approach. While the Monte Carlo model may be necessary for complex structured targets, this model can provide a quick, accurate prediction of the bremsstrahlung background from elemental, molecular or layered targets. The results of the present model can be compared with Monte Carlo calculations, which can serve as quasi-experiment, and also with actual absolute bremsstrahlung yield experiments. Furthermore, this model can help us to evaluate and understand the importance of the various physical processes involved in bremsstrahlung production, such as electron backscattering, photon attenuation and electron multiple scattering. This model will also be useful in describing the bremsstrahlung background in PIXE and proton microprobe experiments. In ion beam bombardment the background comes from secondary electron bremsstrahlung. Hence this model, which provides the bremsstrahlung spectrum from a mono-energetic electron, provides needed input data for the calculation of bremsstrahlung from ion bombardment in which the model bremsstrahlung spectrum is integrated over the secondary electron spectrum produced by binary collisions with the incident ion. Finally, this model should be useful in diverse areas where electron bremsstrahlung is important such as in the interaction of solar wind with planetary atmosphere, or the production of bremsstrahlung in plasmas where the bremsstrahlung spectrum is used as a diagnostic tool.

The first consideration of thick-target bremsstrahlung was by Kramers[1] in 1923. Kramers used a classical calculation for the single interaction of an electron with a target atom and used the Thomson–Whiddington law to compute the electron energy loss and integrate the probability of radiating over the energy of the electron as it comes to rest in the target.

*Correspondence to: C. A. Quarles, Department of Physics, Texas Christian University, TCU Box 298840, Fort Worth, Texas 76129, USA. Email: c.quarles@tcu.edu

XRS

Kramers obtained a simple dependence for the radiation spectrum before any corrections for electron scattering in the target or x-ray self-attenuation. The Kramers equation for the radiated energy distribution from a target atom of atomic number Z is

$$I(Z, E_0, E_v) = \text{constant} \times Z(E_0 - E_v) \quad (1)$$

This simple equation illustrates the essential features of the energy radiated at x-ray energy E_v from a monoenergetic incident electron of energy E_0. The energy radiated depends linearly on Z, unlike the single interaction cross-section that varies as Z.[2] The energy spectrum is linear in x-ray energy and goes to zero at the kinematic end-point E_0 (the Duane–Hunt limit). Correction of this equation for self-attenuation in the target produces the familiar energy dependence of the thick-target bremsstrahlung spectrum rising linearly from the end-point energy to a peak and then falling off at low x-ray energy due to increasing attenuation.

Many efforts have been made over the years to develop a physical model of the process that improves on the simple Kramers equation. A significant effort to improve on Eqn (1) was due to Storm.[2] He compared Eqn (1), which he called the Kramers–Kulenkampff–Dyson (KKD) equation when the constant is specified, with the bremsstrahlung energy spectra based on two thin-target bremsstrahlung equations given by Koch and Motz[3] in their milestone review. Storm discussed many aspects of the problem in considerable detail. Storm used energy spectra that, like Eqn (1), either did not contain any angular dependence or could be considered an average over emission angle. Interestingly, Storm concluded that the uncertainties in the electron backscattering and neglect of the angular dependence as well as uncertainties in the measurements precluded any selection among the various bremsstrahlung theories. He also proposed semi-empirical results that were in agreement with most experiments at the level of about 20%.

Ambrose *et al*.[4] extended Storm's model by using the relativistic partial-wave thin-target bremsstrahlung cross-sections tabulated by Kissel *et al*.[5] Ambrose *et al*. applied the model to the case of the bremsstrahlung produced in transmission by 70 keV electrons (from a small Cockcroft–Walton electron accelerator) on a variety of target foils with Z ranging from 6 to 92. The targets were thick enough to stop the electron beam, but thin enough to transmit the x-ray spectrum. Transmission angles of 45° and 90° were studied. The angular dependence was explicitly exhibited. Comparisons were made with both the KKD model of Storm and the model using the tabulated bremsstrahlung spectrum,[5] referred to as KQP. The data at 45° were well described by the KQP model both in x-ray energy dependence (shape) and in absolute scale (to about 20%). The data at 90° were described well in shape but the intensity was 30–70% higher than the model prediction. This suggested that at 90° the emission angle of the x-ray had been effectively averaged by electron scattering in the target. The intensity was, on average, higher than that from 90° emission alone. The self-absorption in the transmission case was dominated by the total thickness of the foils and so was not affected by the uncertainty in the location of origin of the x-ray. The correction for electron backscattering was made by extending the approach used by Storm for tungsten to other atomic numbers.

In the present work, the model of Ambrose *et al*.[4] was applied to describe the continuum spectra from an SEM. Good results for the shape of the bremsstrahlung were obtained with the model for target atomic numbers ranging from 4 to 79 and for electron energies from 5 to 25 keV. While an effort has been made to put as much physics into the model as possible, the model is still semi-empirical since the attenuation factor is allowed to vary from the purely geometric factor expected from the SEM detector geometry to obtain a better fit to the data. The backscattering correction was used by Ambrose *et al*.,[4] but it too is a semi-empirical correction since it is applied as an overall correction whose x-ray energy dependence is approximate. The model, however, is found to be as good as recent empirical models[6] at predicting the shape of the bremsstrahlung spectrum.

DETAILS OF THE MODEL

The essential idea of the model is to integrate the thin-target bremsstrahlung spectrum produced by the electron as it slows down in the thick target. The Bethe continuous slowing down approximation as tabulated by Berger and Seltzer[7] was used to evaluate the $\mathrm{d}E/\mathrm{d}x$ of the electron as a function of energy E.

The x-ray energy distribution detected at angle θ relative to the incident electron beam, at energy E_v from an electron with incident energy E_0 is given by

$$I(Z, E_0, E_v, \theta) = \varepsilon R \int_{E>E_v}^{E_0} E_v \frac{\mathrm{d}\sigma}{\mathrm{d}\Omega \mathrm{d}E_v} \frac{\mathrm{d}E}{(-\mathrm{d}E/\mathrm{d}x)} \times \exp\left[-\mu(Z, E_v)x\xi\right] \quad (4)$$

where $\mathrm{d}\sigma/\mathrm{d}\Omega\mathrm{d}E_v$ is the bremsstrahlung doubly differential cross-section from the KQP tabulation.[5] The tabulated cross-section is a function of Z, E_0, E_v and θ, R is the electron backscattering correction and ε is the detector efficiency. To include electron energy loss, the integral is taken from the radiated x-ray energy E_v to the incident electron energy, or the maximum x-ray energy, E_0.

The exponential factor in Eqn (4) corrects for self-attenuation in the target. $\mu(Z, E_v)$ is the x-ray absorption coefficient for the target, which is available from tabulations.[8] ξ is a geometric factor nominally given by $\xi = 1/\cos(180° - \theta)$. For an x-ray emission angle of 130°, $\xi = 1.55$.

However, in the model, ξ has been allowed to vary from this simple geometric factor to obtain a better fit. The variation is plausible since the electron does not follow a straight path in slowing down in the target. Rather the electron multiply scatters as it slows down. Thus the average distribution of the electron distances is less than what would be expected from a strict linear path. ξ has been found to vary with Z from about 0.8 to 0.5 as Z varies from 4 for Be to 79 for Au. This dependence is also plausible since both multiple scattering and backscattering increase with Z.

$\mathrm{d}E/\mathrm{d}x$ in Eqn (4) is calculated from the tables of Berger and Seltzer.[7] A subprogram was written to return the value

of x for any E and correspondingly E for any x in the target to facilitate the calculation.

R is the backscattering correction. This factor is based on the correction developed by Storm for tungsten. The correction was extended by Ambrose *et al*.[4] to have the same E_ν dependence, but depend on the total backscattering factor $\eta(E_0, Z)$:

$$R = \frac{1 - \eta(E_0, Z)}{1 - \eta(E_0, Z)\dfrac{E_\nu^2}{E_0^2}} \tag{5}$$

where $\eta(E_0, Z)$, given by August and Wernisch,[9] varies slowly with Z and is almost independent of E_0:

$$\eta(Z, E_0) = E_0^{\left(0.1382 - \frac{0.9211}{\sqrt{Z}}\right)}[0.1904 - 0.2236\log Z + 0.1292(\log Z)^2 - 0.01491(\log Z)^3] \times [0.9987 + 2.167 \times 10^{-4} Z] \tag{6}$$

The detector efficiency ε in Eqn (4) is modeled by

$$\varepsilon = \exp(-\mu_{Be}x_{Be} - \mu_{Au}x_{Au} - \mu_{DL}x_{DL}) \times [1 - \exp(\mu_{Si}x_{Si})] \tag{7}$$

In the first exponential the μ's and x's are the photon absorption coefficient and thickness for the Be window, the Au detector contact layer or the silicon dead layer (DL) including any surface ice layer. Unfortunately, the SEM used has an Oxford Instruments Link detector made in 1990, and it was not possible to obtain information about the contact layer (apparently it is not Au or only Au) or the silicon dead layer as this information is still considered proprietary. However, the assumption of an 'effective gold layer' and an 'effective Si dead layer and ice layer' is reasonable. We used an effective Au contact layer thickness of 0.01 μm and an effective silicon dead layer of 0.1 μm that are typical for detectors of this sort. In fact, there is always going to be some uncertainty in the absorption since the ice layer is not well known and can vary over time. Interestingly, the fit is improved somewhat with assumption of a smaller 'Au layer.' In the second exponential factor in Eqn (7), μ_{Si} is the absorption coefficient for silicon and the x_{Si} is the detector thickness (3 mm).

INSTRUMENTATION

The instrument is a Jeol JSM 6100 SEM with a 3 mm thick Si(Li) detector with a 0.008 mm Be window. These factors are used to calculate the detector efficiency discussed above. The take-off angle is nominally 50°, which corresponds to an x-ray emission angle of 130° with respect to the incident electron beam direction. The solid angle and beam current have not been measured. In this work we concentrated on the shape of the bremsstrahlung, not on the absolute intensity. With the SEM used, it was not possible to measure the absolute beam current; however, we hope to obtain absolute intensity values in future experiments in a different experimental setup.

RESULTS AND DISCUSSION

Typical results are shown in Figs 1 and 2. The x-ray energy distribution per incident electron, $I(Z, E_0, E_\nu, \theta)$ from Eqn (4), is plotted versus x-ray energy. As can be seen from Eqn (4), the units of I are the product of energy (in keV), the differential cross-section (in $cm^2\ keV^{-1}\ sr^{-1}$) and thickness (in atoms cm^{-2}) or simply sr^{-1}. We plot the results scaled by Z^{-1} to put the data from different atomic number targets on about the same scale since I is expected to be approximately proportional to Z [Eqn (1)]. The data have been normalized to the model. The data were collected in typically 1 h runs with a fixed beam current and magnification set at 1000. The beam intensity is stable over several hours and does not change with the magnification, but variations in the rate of a few percent have been observed in repeated short runs. The model evaluates the spectrum from 2 keV to the end-point. We have not evaluated below 2 keV since the x-ray absorption coefficients are only tabulated with reliability above 1 keV. Certainly in the future it would be interesting to extend the model below 1 keV.

The fits generally can be seen to be good, although there are a few areas of systematic difference. The data at high Z seem to be generally better described than the low-Z data. At low Z the lower energy data (Al at 25 keV in Fig. 1 and Be at 15 keV in Fig. 2) seem to be more attenuated by self-absorption than the theory suggests. In the intermediate Z region, for example Cu (not shown), or Ni at 25 keV in Fig. 1, the data are significantly lower than the model at energies just below the characteristic x-rays, again suggesting that there is more self-absorption in this case than the model predicts. No manipulation of the parameters of the model could compensate for this effect.

Of course, it should be pointed out that better fits for any individual spectrum can be obtained by varying the parameters of absorption and backscattering. However, it was not our purpose here to produce another empirical fit to data. Rather, we were interested in exploring what features of the physical model need to be considered to improve the model over a wide range of beam energy and atomic number.

Figure 3 illustrates the effect of the assumption of a fixed emission angle or average emission angle on the spectrum shape for Au and Al at 25 keV. The solid curves are the theory for a fixed emission angle of 130° and the dotted curves assume an average emission angle or isotropic photon emission. For both targets, the upper curves are the theory without inclusion of backscattering or absorption and the lower curves include these effects. For the case of an average emission angle (dotted curves) we use the bremsstrahlung energy spectrum of Kissel *et al*.[5] and assume an isotropic emission. This average angle approach was used by Storm.[2] However, using the actual emission angle improved the model in the earlier study in transmission mode at 45° and 90°. From Fig. 3 we can see that there is a difference in the photon energy dependence depending on the emission angle assumption. For higher photon energies, the average emission angle theory predicts a lower intensity, whereas for low photon energy, the average angle theory predicts a higher intensity. This difference in the prediction of the two theories can also be seen in the spectra including backscattering and absorption. The actual data spectra (Figs 1 and 2) are better fitted in the high photon energy region by

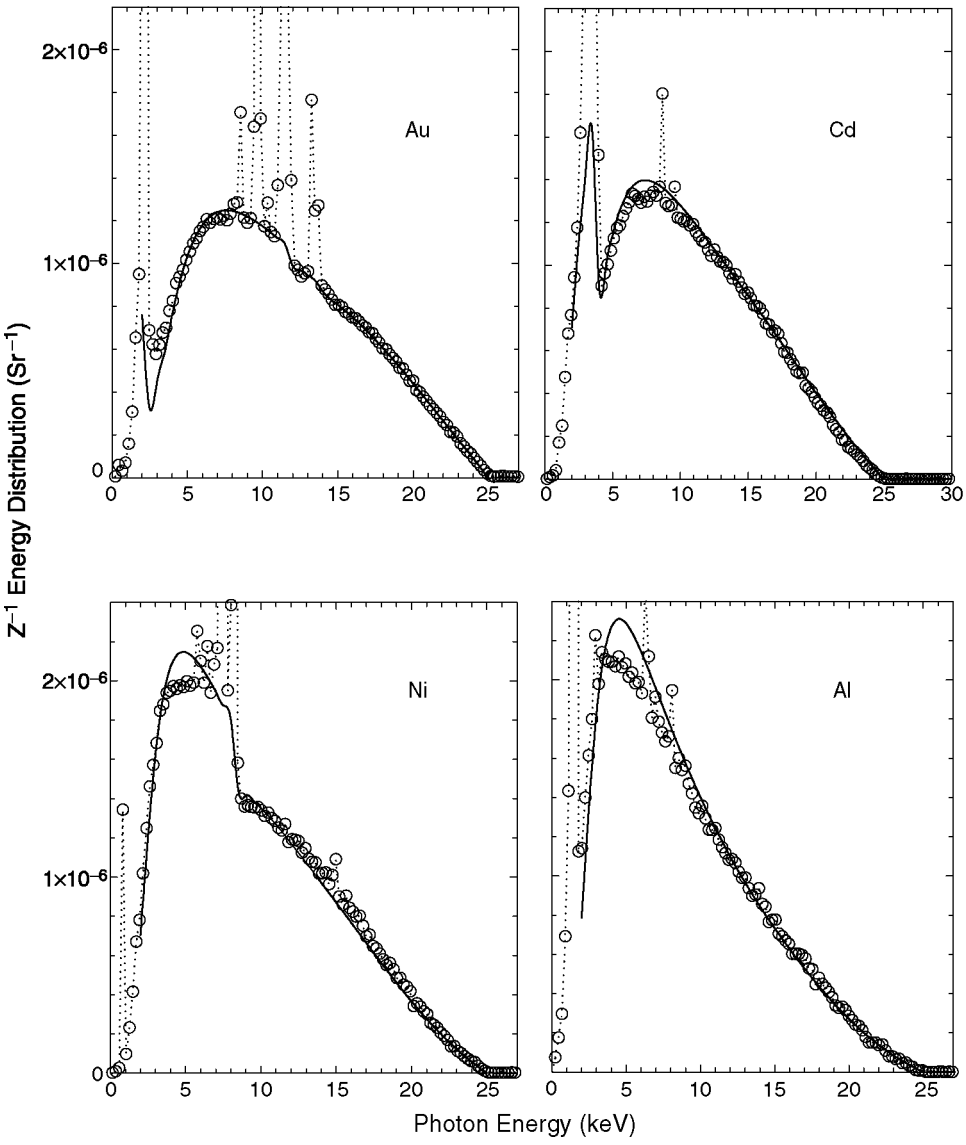

Figure 1. Typical results for the x-ray energy distribution from Eqn (4) in units of sr^{-1} for 25 keV electrons on targets of Au, Cd, Ni and Al. The data have been normalized to the model.

the fixed emission angle assumption. This is as expected since the higher energy photons must be produced before the electron has penetrated the target or multiply scattered much. Also note that there is a change in the shape of the spectrum for the 130° emission from concave upward to concave downward on going from low to high Z. For certain intermediate Zs the spectrum would be almost linear with photon energy until the backscattering and absorption become dominant.

In Fig. 4 we illustrate the average effects of backscattering, absorption and detector response for Au and Al targets. The detector response, of course, is independent of the target, and for a 3 mm thick detector has a significant effect above about 15 keV. Over the range from about 5 to 15 keV, however, both the detector response and absorption corrections are small. In this region the major effect is the treatment of backscattering. As can be seen, the effects of backscattering and absorption are much more important for the high-Z target. Hence the thick-target spectrum from a low-Z target will continue to reflect the thin-target theory better than the spectrum from a high-Z target. Perhaps this is the reason why Storm was unable to distinguish among various thin-target theories with data from a W target. If we are interested in using the thick-target spectra to investigate differences in the thin-target theory, it is better to concentrate on low-Z targets which are less affected by uncertainties in the backscattering or absorption corrections.

Finally, as an interesting example of what one can do with the present model, Fig. 5 shows the results for a 'hybrid' calculation for Al and Au targets at 25 keV using a version of the model that combines the features of both fixed and average emission angle. At 0.4 times the beam energy (somewhat arbitrarily chosen), the model switches from fixed angle to average angle, normalizing the average-angle theory to the fixed-angle theory at that point. The result (compare Fig. 1 with Fig. 5) is to improve the low-energy behavior of the model while retaining the good fit at high photon energy that is characteristic of the fixed-angle model. This also illustrates that the model can be improved by approximating more of the actual physics of the process since as the electron

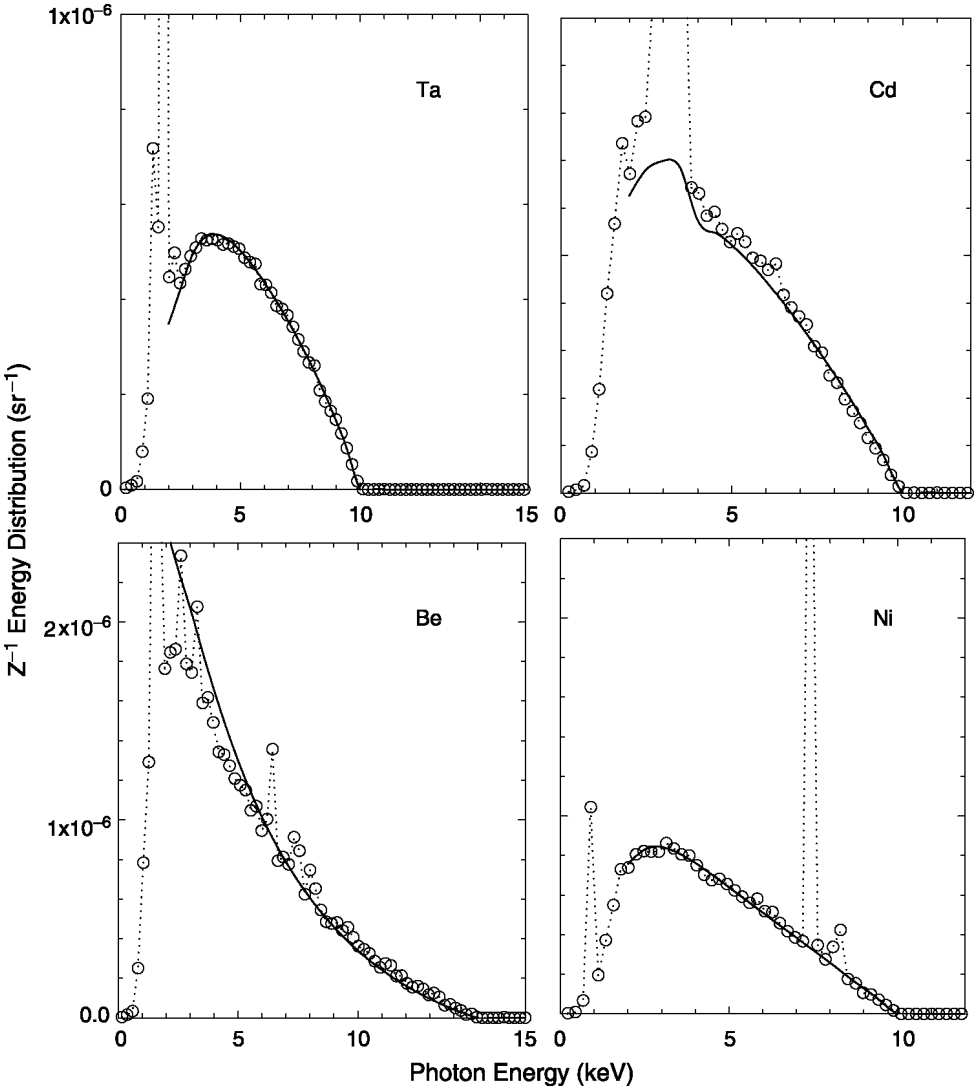

Figure 2. Typical results for the x-ray energy distribution from Eqn (4) in units of sr^{-1} for 10 and 15 keV electrons on targets of Ta, Cd, Ni and Be. The data have been normalized to the model.

loses energy in the target it multiply scatters and thus the emission angle becomes more randomized.

The results presented in Figs 1 and 2 for the energy dependence of the energy distribution compare favorably with semi-empirical models. Trincavelli *et al*.[6] discussed and compared their recent work in developing a better semi-empirical model with earlier efforts to describe the energy distribution.[10–12] One of the main differences in the present model is the use of the best available single-atom cross-sections in the calculation of the integrated spectrum from a thick target [Eqn (4)]. Thus the deviation from the simple linear Z dependence comes naturally from the use of more exact cross-sections and does not need to be added as an empirical correction term. As an alternative to semi-empirical modeling, the Monte Carlo approach has always been taxing owing to the small cross-section for radiation compared with elastic scattering and ionization. However, some promising recent progress has been reported. Preliminary Monte Carlo results with the Sesame program by Schiebl and co-workers[13,14] using the KQP cross-sections[5] have shown fair agreement with SEM data. However, they are not yet able to reproduce the absolute intensities as well as had been hoped. The present model agrees well with the shape of the spectrum predicted by the Sesame Monte Carlo model. Another recent Monte Carlo approach by Acosta *et al*.[15] uses the PENELOPE program. The authors developed an effective sampling method that reproduces the thin-target KQP cross-sections of Kissel *et al*.[5] Results for Cu and Ag at 20 keV from an electron microprobe, as well as other cases, are well reproduced by the Monte Carlo calculation both in spectrum shape and in absolute intensity.

CONCLUSIONS

We have obtained a good description of the photon energy dependence or shape of the bremsstrahlung spectrum from 10 to 25 keV electrons on targets with atomic numbers ranging from 4 to 79 in a reflection (SEM or EPMA) geometry. Since the beam current was not measured in the present setup, it is not possible to comment on the agreement of the model with the *absolute* scale of the data. However, a good physical model of the continuum background spectrum that

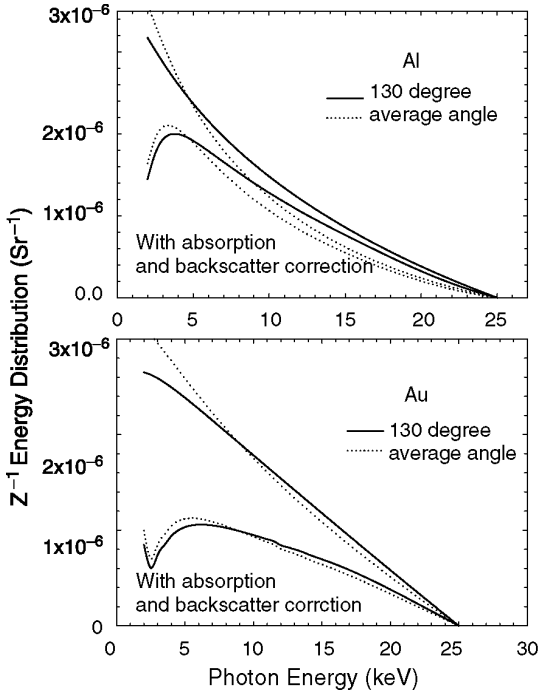

Figure 3. X-ray energy distribution from Eqn (4) for 130° emission angle (solid line) and for average emission angle (dotted line) for Au and Al at 25 keV. In each plot the upper curves are the energy distribution computed using the KQP thin-target cross-sections[5] without correction for electron backscattering and self-absorption. The lower curves include corrections for self-absorption and backscattering.

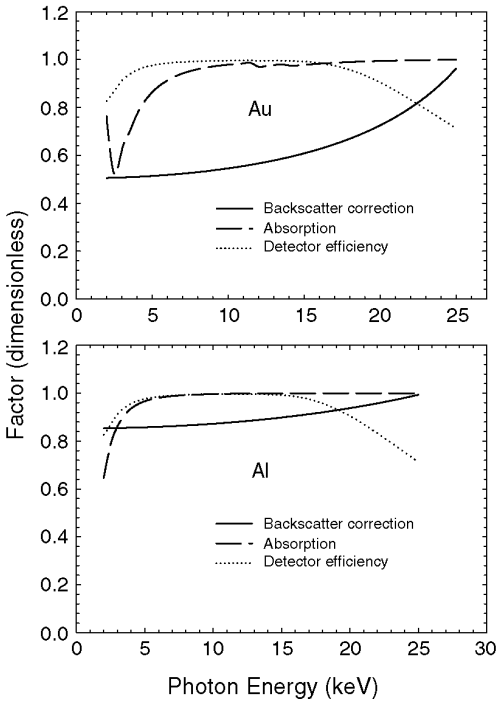

Figure 4. The backscattering correction factor, self-absorption correction factor and detector efficiency for Au and Al for 25 keV electrons.

is based on the best available single-atom bremsstrahlung cross-sections should be useful in an SEM or EPMA in the

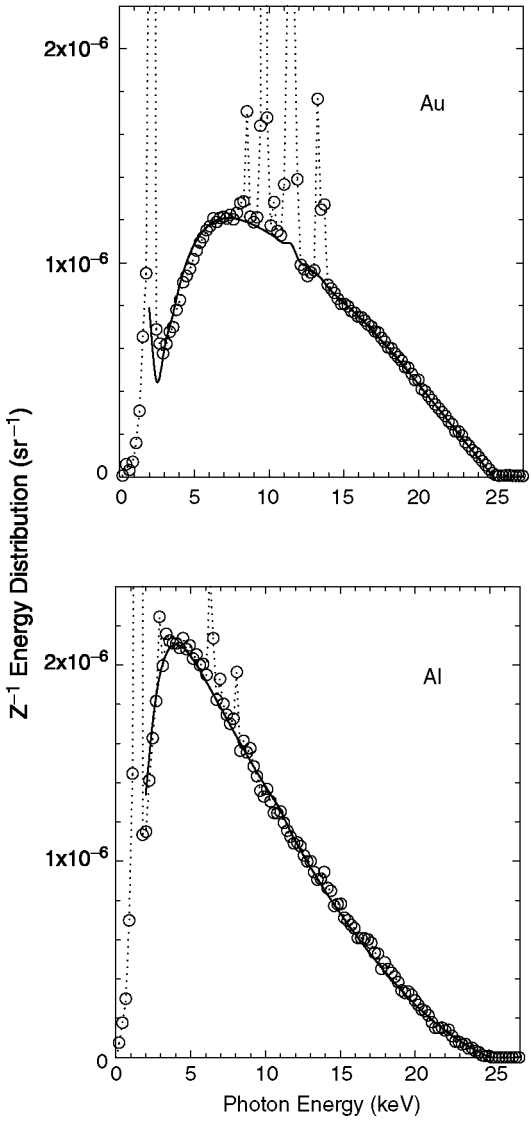

Figure 5. Illustration of the improved fit using the 'hybrid' model that switches from a fixed emission angle of 130° to an average emission angle at 0.4 times the incident electron energy. The improvement in the fit is more evident for the Al case when compared with Fig. 1, but there is also improvement in the Au fit, especially just below the L characteristic x-rays.

extraction of more accurate characteristic x-ray intensities. The model described here can be evaluated for any energy and target and the results can be simply scaled to the data at a convenient energy higher than the characteristic x-ray of interest. The model can be extended to include targets that are molecules or mixtures of atoms.

In a future experiment planned for a small electron accelerator, absolute yields will be obtained for comparison with the model. In the previous use of this model,[4] good agreement was found with the absolute yield for a photon emission angle of 45°, but the emission at 90° was 30–70% low so further study of the absolute yield, particularly at backward angles characteristic of the SEM geometry, is important. It may prove necessary to modify the model as illustrated in Fig. 5 to average over the emission angle in order to take account of the electron scattering in the target.

Secondary electron effects have so far been neglected in the model. Additional study of the backscattering correction and self-absorption may also be needed.

REFERENCES

1. Kramers H. *Philos. Mag.* 1923; **46**: 836.
2. Storm E. *Phys. Rev. A* 1972; **5**: 2328.
3. Koch HW, Motz JW. *Rev. Mod. Phys.* 1959; **31**: 920.
4. Ambrose R, Kahler DL, Lehtihet HE, Quarles CA. *Nucl. Instrum. Methods Phys. Res. B* 1991; **56/57**: 327.
5. Kissel L, Quarles CA, Pratt RH. *At. Data Nucl. Data Tables* 1983; **28**: 381.
6. Trincavelli J, Castellano G, Riveros JA. *X-Ray Spectrom.* 1998; **27**: 81.
7. Berger MJ, Seltzer SM. NASA SP 3012, 1964, Current Tabulation on the Web: Program ESTAR. http://physics.nist.gov/PhysRefData/Star/Text/ESTAR.html. [17 December 2000].
8. Storm E, Israel HI. *Nucl. Data Tables* 1970; **7**: 565. Current Tabulation on the Web: XCOM: Photon Cross Sections Database, NIST Standard Reference Database 8 (XGAM), NBSIR 87-3597. http://physics.nist.gov/PhysRefData/Xcom/Text/XCOM.html. [17 December 2000].
9. August HJ, Wernisch J. *Phys. Status Solidi A* 1989; **114**: 629.
10. Fiori CE, Myklebust R, Heinrich K, Yakowitz H. *Anal. Chem.* 1976; **48**: 233.
11. Small J, Leigh S, Newbury D, Myklebust R. *J. Appl. Phys.* 1987; **61**: 2, 459.
12. Goldstein JI *et al.* (eds). *Scanning Electron Microscopy and X-Ray Microanalysis: a Text for Biologists, Material Scientists and Geologists*, Plenum Press: New York, 1992.
13. Schiebl CO, Ambrose V, Wernisch J. In *Microscopy and Microanalysis. Proceedings: Microscopy & Microanalysis '99, Portland, Oregon, August 1–2, 1999*, vol. 5, suppl. 2, G. W. Bailey, W. G. Jerome, S. McKernan, J. F. Mansfield, R. L. Price (eds). Springer: New York, 1999; 82.
14. Schiebl CO, Ambrose V. In *Microscopy and Microanalysis. Proceedings: Microscopy & Microanalysis '99, Portland, Oregon, August 1–2, 1999*, vol. 5, suppl. 2, G. W. Bailey, W. G. Jerome, S. McKernan, J. F. Mansfield, R. L. Price (eds). Springer: New York, 1999; 608.
15. Acosta E, Llovet X, Coleoni E, Riveros JA, Salvat F. *J. Appl. Phys.* 1998; **83**: 6038.